Cryogenics xxx (2008) xxx–xxx

Contents lists available at ScienceDirect

Cryogenics

journal homepage: www.elsevier.com/locate/cryogenics

Microstructural factors important for the development of high critical current density Nb_3Sn strand

Peter J. Lee [a,*], David C. Larbalestier [b,1]

[a] The Applied Superconductivity Center, National High Magnetic Field Laboratory, Florida State University, 251 Shaw Building, 2031 E. Paul Dirac Dr. Tallahassee, FL 32310-3711, United States

[b] The Applied Superconductivity Center, National High Magnetic Field Laboratory, Florida State University, 252 Shaw Building, 2031 E. Paul Dirac Dr. Tallahassee, FL 32310-3711, United States

ARTICLE INFO

Available online xxxx

Keywords:
A. Superconductors
A. Metals
C. Critical current density
C. Critical field
C. Critical temperature

ABSTRACT

Nb_3Sn is the primary candidate for the next generation of accelerator magnets as well as for NMR and other applications that require magnetic fields between 11 and 20 T. Since 1999 the layer critical current density available in long length accelerator quality strand has almost doubled. The microstructural and microchemical factors that are important for high critical current density Nb_3Sn are reviewed. The highest critical current density strands have a Nb_3Sn layer that minimizes chemical and microstructural inhomogeneities and has a high fraction of the layer close to stoichiometric Sn content. Only the internal Sn process has yielded critical current densities beyond 3000 A/mm^2 at 12 T (4.2 K) and only with interfilamentary Cu thicknesses that are too low to separate the filaments after the final reaction heat treatment. The result of the reaction heat treatment is to produce a continuous ring of Nb_3Sn from hundreds of Nb or Nb-alloy filaments and thus a major ongoing challenge of Nb_3Sn conductor design is to reduce the effective filament diameter to acceptable levels for intended applications. Recent successful attempts to reduce the cost of alloying the Nb_3Sn for high field application are also examined and the potential for future improvements discussed.

1. Introduction

The demands of the high energy physics community for higher-field, engineering-quality superconductors for accelerator applications continue to drive superconducting strand technology to higher critical current densities at high magnetic fields. A comparison of critical current densities for long length superconducting strands at applied magnetic fields above 10 T is shown in Fig. 1. Typically accelerator magnet builders target a non-stabilizer critical current density of 1000 A/mm^2 or more, which limits the application of Nb–Ti (as used for the LHC) to fields below ~11 T. The huge potential of the round wire multifilament HTS superconductor Bi-2212 for high fields is clear from this comparison, providing that a reliable conductor-magnet technology can be developed. Two A15 superconductors, Nb_3Sn and Nb_3Al, are available in conductor form and push the available field well beyond 12 T. The development of high performance Nb_3Al strand is reviewed elsewhere in this publication [1]. Nb_3Sn technology has also been the subject of a recent historical review by Suenaga [2] and aspects of the A15 composition, grain morphology and strain state have recently been reviewed by Godeke [3]. Summarizing broadly, we can say that Nb_3Sn strand fabricated using a high Sn bronze matrix does not provide sufficiently high Sn contents (9–10 at.%Sn for a homogeneous and ductile bronze) to avoid large Nb_3Sn A15 phase composition gradients across the A15 layer. These gradients in turn produce large gradients in the superconducting properties that limit the overall current density, especially at high fields, even though long lengths of commercial bronze strands are produced with the excellent filament size, spacing and geometric uniformity required by demanding NMR applications. Powder-in-Tube (PIT) based strands based on the ECN process [4] were the first Nb_3Sn strands to be successfully incorporated into an accelerator dipole that could clearly work in the field and temperature domain not accessible to Nb–Ti [5] and to show that non-stabilizer critical current density (J_c) values beyond 2000 A/mm^2 at 12 T (4.2 K) could be reached [6]. The PIT technique is extensively reviewed by Godeke elsewhere in this journal [7], while here we concentrate mainly on characterizations that we have made of the Internal Sn (IT) Process wires. Earlier work of ours in the 1999–2004 time frame on the PIT wires led us to important conclusions about the way that radial inhomogeneities produced by the Sn diffusion step needed to form the Nb_3Sn affect the properties of wires. These inhomogeneities are present in all filamentary conductor designs [8], but to

* Corresponding author. Fax: +1 850 645 7754.
E-mail addresses: lee@asc.magnet.fsu.edu (P.J. Lee), larbalestier@asc.magnet.fsu.edu (D.C. Larbalestier).
[1] Fax: +1 850 645 7754.

0011-2275/$ - see front matter © 2008 Elsevier Ltd. All rights reserved.
doi:10.1016/j.cryogenics.2008.04.005

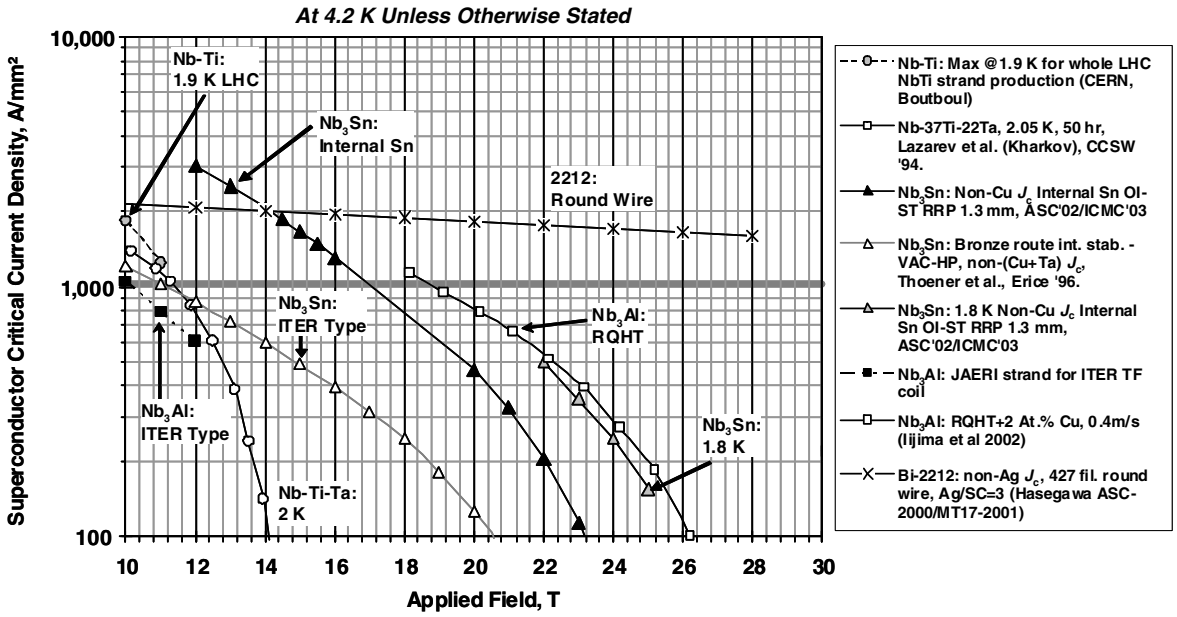

Fig. 1. Variation in superconductor critical current density normalized either to the superconductor cross-section (Nb–Ti, Bi-2212) or to the package required to make the superconductor (Nb_3Sn, Nb_3Al) with applied magnetic field above 10 T for engineering superconductors. For accelerator application the critical current density should exceed 1000 A/mm^2.

different extents depending on the exact architecture of each wire. They appear less clearly in many IT wires, but still remain decisive for the wire performance.

The IT process was developed to avoid frequent in-process annealing during wire drawing and to enhance the available Sn concentration with respect to the bronze process by using separate Sn, Cu and Nb billet stacking elements rather than specially melted high Sn, P-free bronze matrix alloys [9]. By 1998 both IGC-AS [10], using stacked rods of Nb in tubes of Cu around each Sn source, and OI-ST, using the Modified Jelly Roll (MJR) process [11] (an expanded slit sheet of Nb is co-rolled into a sub-element coil with a sheet of Cu that provides the matrix), had produced Nb_3Sn strand giving 2200 A/mm^2 (measured over the total non-stabilizer Cu fraction, including Nb or Ta diffusion barrier) at 12 T (4.2 K).

1.1. The US conductor development program

This promise of much higher critical current density was of particular interest to the builders of next generation particle accelerator magnets. In 1999 a conductor development program (CDP) was initiated by the US Department of Energy Office of High Energy Physics as a driver to push strand technology to lower cost and higher performance for this next generation of accelerator magnets beyond the LHC [12]. The initial target specifications, recognized to be very ambitious, outlined by the CDP were

1. Critical current density, J_c (non-copper, l2 T,4.2 K) > 3000 A/mm^2.
2. An effective filament size (D_{eff}) of less than 40 μm.
3. Average wire piece lengths >10 km.
4. Wire cost <$1.5/kA m (4.2 K, 12 T).

Although no Nb_3Sn strand had been manufactured with J_c (12 T, 4.2 K, 10 μV/m) values beyond 2200 A/mm^2 at that time, there was indeed reason to hope that 3000 A/mm^2 was possible. There had been a 50% increase in reported in layer J_c values for high Sn strand compared to ITER Model Coil strand [13], 5100 A/mm^2 had been derived from recent developmental composites [14] and 7000 A/mm^2 had been obtained for tin films of Nb_3Sn containing fine precipitates by Dietderich and Scanlan [15]. Initial efforts were focused on the J_c (12 T, 4.2 K, 10 μV/m) target (unless otherwise explicitly stated, all J_c values in this paper are for this condition) but cost saving technologies (especially including technologies that benefited scale-up to larger billets) were also encouraged in parallel both through the CDP and the DOE-SBIR program. The cost factors associated with engineering strands of various designs have been the subject of a recent topical review by Cooley et al. [16].

1.2. Rapid development of high J_c strand

An important benefit of the IT process is that billets with realistic filament architectures can be quickly constructed from simple constituents, principally Sn, Nb and Cu, on a small scale, making the R&D cycle quite rapid. With the Sn:Nb ratio set high enough to provide more than sufficient Sn for full stoichiometric reaction, thus leaving some residual Sn in the Cu(Sn), an important remaining variable is the Cu content of the Nb:Sn:Cu sub-element pack. It was expected that reducing the Cu between Nb sub-elements would increase D_{eff} but with J_c as the primary goal this compromise or design drawback was chosen as the most accessible route to very high J_c. The MJR design allowed OI-ST to quickly reduce the interfilamentary Cu in their trial composites and progress was rapid with 2900 A/mm^2 reported in 2001 [17,18]. Reducing the Cu in the filament pack resulted in a substantial increase in the Sn:Cu ratio, such that it was now similar to the 27 at.%Sn-in-Cu mixture for tin-in-tube-process strands reported in 1979 [19]. In this pioneering work by Murase and co-workers, not always well remembered in recent years, it was found that increasing the Sn content beyond about 27 at.% resulted in melting of the Sn–Cu at their reaction temperature of 700 °C, dissolution of some Nb and a decline in J_c. Similar dissolution of the inner Nb filaments in an MJR composite was observed by Naus et al. [20] and degradation of J_c at very high Nb contents was rediscovered during the optimization of recent IT strands [18]. Indeed the dissolution of Nb filaments by the very corrosive Sn–Cu liquid phase places an important lower limit on the amount of Cu needed in the filament pack [18,21].

Please cite this article in press as: Lee PJ, Larbalestier DC, Microstructural factors important for the development of high critical current ...., Cryogenics (2008), doi:10.1016/j.cryogenics.2008.04.005

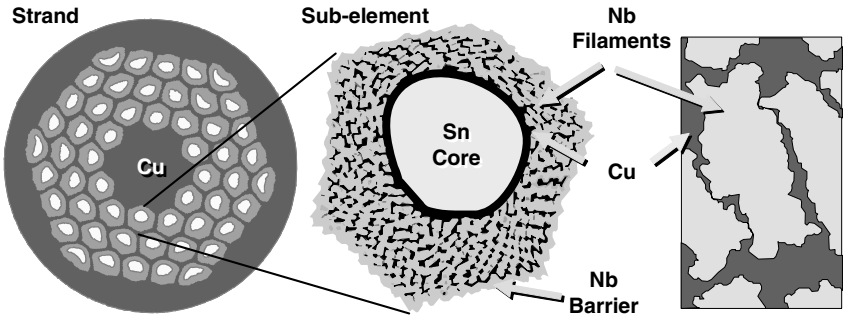

Fig. 2. Schematic illustration of an unreacted cross-section of a high J_c internal Sn MJR composite with Nb diffusion barrier wraps around each sub-element. The Sn core and the Nb filaments may be alloyed.

The high J_c MJR composite design (illustrated schematically in Fig. 2) has multiple sub-elements organized into bundles, each bundle being surrounded with a Nb diffusion barrier which reacts partially to Nb_3Sn during reaction heat treatment and contributes to the superconductor cross-section and thus J_c but less desirably also to the hysteretic coupling loss and, when too thin, also allows leakage of Sn into the stabilizing Cu, producing a poisoning, that under the worst of circumstances, leads to magnet flux jumps and premature quenching [22]. Recent modeling of magneto-thermal instability that incorporates self field effects provides good agreement with experimental data for MJR strands [23]. In 2001 OI-ST introduced their Restacked Rod Process (RRP), which used Nb rod extrusions with a Cu sheath that could be reduced to very small thickness. Because this allows billet scale-up with one extrusion step, this technique has now replaced the MJR process at OI-ST.

IGC-AS in Waterbury, CT, (now Luvata-AS) had been using Nb-rods inserted into a carefully designed array of gun drilled holes in a Cu sub-element billet for their low hysteresis loss strands but the local area ratio (LAR) of Cu/Nb for this method was limited to 35/65 [24]. By switching to a round-array, Cu-sheathed Nb process they found it became possible to reduce the Cu content to below 18 vol.%. As Outokumpu Advanced Superconductors (OKAS), the Waterbury group soon increased the performance of this design to a non-stabilizer J_c of ~2600 A/mm^2 at 12 T [25]. The fabrication route for the Waterbury high J_c strand started with a 20/80 local area ratio (LAR) of Cu to Nb-rods stacked into a 179 mm diameter billet. After extrusion and Sn insertion into their cores, the sub-element rods were drawn and restacked with a single Ta diffusion barrier around the sub-elements and stabilizer Cu tube outside the barrier [26]. The single Ta barrier is more volume efficient than a barrier around each sub-element but the additional Cu required to separate the bundles of sub-element stacks inside the barrier makes it more difficult to achieve high Sn:Cu ratios with the reaction package.

These rapid advances in Nb_3Sn performance have translated into dramatic increases in the highest fields produced in prototype accelerator magnets. In 2001 LBNL pushed the record high field in a prototype accelerator magnet to 14.7 T using 2000 A/mm^2 class strand from OI-ST [27]. By using the new OI-ST RRP high J_c strands with 15 T (4.2 K) critical current densities greater than 1450 A/mm^2, the LBNL Superconducting Magnet Group were able to increase the record field to 16 T in a block coil design in October 2003 [28].

1.3. The influence of microchemistry on intrinsic properties

The maximization of J_c in Nb_3Sn conductors is a complex compromise between the amount of A15 phase in the cross-section, since the J_c is averaged over the whole package needed to produce the A15 phase (including diffusion barriers), and the quality of the A15. At first it was widely assumed that the principal benefit of the IT design was its ability to produce much higher volume fractions of A15. In fact the difference in A15 content between a 2000 A/mm^2 and a 3000 A/mm^2 strand is relatively small: 60 vol.% in a 2200 A/mm^2 MJR strand compared with 63 vol.% measured for a 2900 A/mm^2 OI-ST rod-in-tube conductor [8]. The crucial difference becomes much clearer when one considers properly the fact that the Nb_3Sn A15 phase field covers a range of composition from 25 to 18 at.%Sn, as determined by studies of bulk compositions [29]. Because it is impossible in any practical conductor to completely convert any Nb filament to a fully stoichiometric A15 with a composition of Nb25 at.%Sn, all filaments have composition gradients that are near stoichiometric at the Sn source-A15 interface and only Nb18 at.%Sn at the A15–Nb interface. A determining index of the quality of the A15 is the nature of this Sn composition gradient across the layer, since the superconducting performance of the filaments is an integration of the radial and longitudinal property variations that the composition (and strain) gradients dictate. A secondary aspect of the quality concerns the density of flux-pinning centers per unit volume. These are principally the grain boundaries, thus making the grain morphology and size also important. As we will see later, there is an important change of morphology that can be correlated to the available Sn that drives the Nb-to-A15 conversion reaction. The basic outline of the great importance of A15 composition to the superconducting properties is indicated in Fig. 3, where the strong dependence of $\mu_0 H_{c2}$ on Sn composition for bulk hot isostatically pressed samples is presented

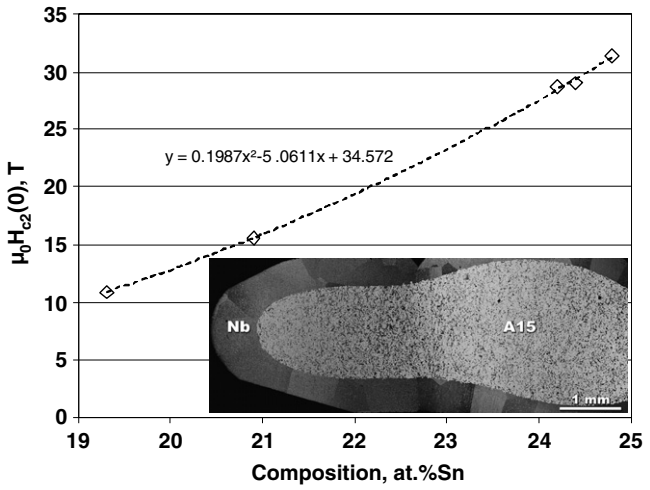

Fig. 3. $\mu_0 H_{c2}(0)$ is an almost linear function of Sn composition for (inset) hot isostatically reacted bulk Nb_3Sn (from the data of Jewell et al. [30]).

from the data of Jewell et al. [30]. The crucial fact is that $H_{c2}(0)$ declines almost linearly from a maximum of ~30 T at the stoichiometric Nb_3Sn composition to ~7 T at the most Sn-poor A15 composition of Nb18 at.%Sn. Always referring to the A15 as the Nb_3Sn layer thus produces a very misleading impression of the quality of A15 layers in Nb_3Sn conductors, though it is almost certainly far too widely used to change.

Study of the quality of the A15 layer has been most direct in the case of PIT conductors because the A15 layer has its lowest T_c on the outside of the filament, making it magnetically transparent to a standard zero-field-cooled T_c transition test and because the layer is thick enough (5–10 μm) for accurate measurement of its composition by electron probe techniques in a scanning electron microscope. High quality PIT conductor became commercially available in the late 1990s when interest in very high J_c designs was renewed. In a series of studies performed in our laboratories, Hawes et al. were able to show substantial agreement between the T_c gradient deduced from magnetization T_c measurements and direct EPMA measurements [31]. It is important to note that even though the Sn gradient declined with increasing heat treatment time, the gradients are never zero, even for extended high temperature heat treatment (110 h at 750 °C). The J_c(H, T) behavior of variously reacted versions of these PIT conductors were then extensively studied by Fischer et al. [32] and then the breadth of the H_{c2}(T) transitions by Godeke et al. Collectively these studies showed that the optimum attainable J_c at a given reaction temperature was a complex balance between minimizing the A15 grain size and minimizing the integrated composition gradient. At 12 T and 4.2 K, it was important to restrict reaction to 675 °C in order to prevent too much grain growth (at 675 °C the mean grain diameter increases from ~110 nm at 8 h to only ~140 nm at 47 h), even though the Kramer extrapolated field H_K (4.2 K) was significantly enhanced from 18.4 T at 8 h to 22.8 T after 47 h and eventually 23.5 T after 128 h at 675 °C. The importance of the gradient was made more generally manifest in a series of radial shell simulations by Cooley et al. [33]. These simulations varied the form of the Sn gradient from linear, as has been generally seen in studies of bronze wires [34–37], to highly non-linear. The conclusion from all of these studies is quite clear. All Nb_3Sn conductors are non-uniform in composition. The non-uniformity is highly dependent on conductor design, especially the Sn–Cu ratio, and on the degree of reaction. Low Sn:Cu ratios induce more linear gradients and greater inhomogeneity. Unlike small-current evaluations of H_{c2}, which tend to seek out the highest H_{c2} fraction in the filament, the Kramer function and its extrapolation provide a weighted mean of the contributions of each radial shell in the filament. Large gradients tend to produce a linearly extrapolated H_K that is below that of the highest T_c and H_{c2} present in the filament [33,38]. Thus ultimate optimization of the conductor must consider the field of prime use, whether at ~0.5H_{c2} where fine grain size still matters, or for very high field use where a better optimization may be provided by a higher temperature reaction which flattens the gradient of Sn, T_c, H_{c2} and J_c(H).

The importance of the Sn:Nb:Cu ratio in the reaction package and the influence that this has on the integrated A15 properties of various IT conductors was investigated by Naus [21], who measured both T_c and the irreversibility field, H^* or equivalently H_K, for a variety of high J_c MJR strands, as well as a PIT strand manufactured by SMI. For a wide range of heat treatments, they found a strong linear relationship between T_c and H^*. An initially rather surprising observation was that many very high J_c strands actually had T_c values of only 16 K. The linear declines seen in Fig. 4 show that T_c and H^* and H_K (and also H_{c2}) are closely coupled, a point which is quite consistent with the subsequent shell modeling of Cooley et al. It is not surprising, then, that large gains in high field critical current can be produced by increasing the Sn content across the entire Nb_3Sn layer. In this respect the IT design has a specific advantage that is possessed by neither the PIT nor the bronze designs, where both conductors retain a discrete filament geometry at all reactions. By contrast the IT design can react such that the filament structure is almost destroyed. For such a high J_c strand, we were able to measure an average radial gradient across the whole A15 layer from core to barrier which was as low as −0.1 at.%Sn/μm [39]. However, quantitative analysis of grain morphology shows that there is still a tendency towards radial columnar growth in towards the centers of the original filaments that make up the high J_c layer. Since columnar grains are almost invariably associated with low Sn content in commercial superconduc-

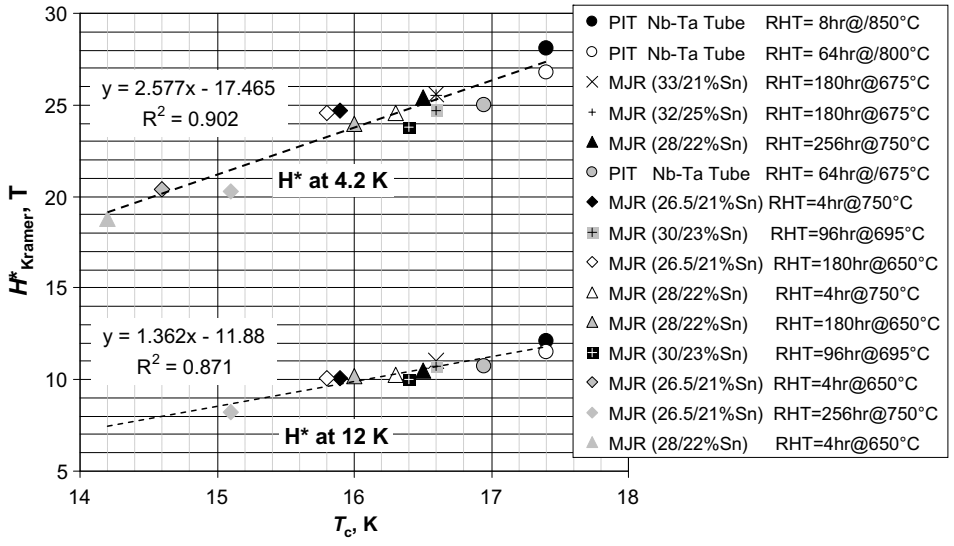

Fig. 4. H^*_{Kramer} at 12 and 4.2 K versus T_c for MJR internal-Sn (Nb–2 at.%Ti filaments, Nb barrier) and PIT (Nb–Ta alloy tubes) composite strands. The legend is sorted by T_c. Two values are given for Sn content in the MJR sub-elements, the first excluding the Nb barrier and the second including the Nb barrier (the barrier is designed to partially react and contribute to superconducting path. The highest 12 T (4.2 K) J_c for these strands, 2900 A/mm^2, was measured for the "32/25%Sn" MJR composite. All the variants fit the linear regression very well. Data courtesy of Michael Naus [21].

Please cite this article in press as: Lee PJ, Larbalestier DC, Microstructural factors important for the development of high critical current ..., Cryogenics (2008), doi:10.1016/j.cryogenics.2008.04.005

tors, their presence indicates that concentric microchemical inhomogeneities can still exist within a low overall gradient. It is interesting here to contrast this behavior with an example where, unlike all commercial superconductors, no Cu is involved in the reaction: For a Ta–Sn/Nb–3.3 at.%Ta tape specimen reacted at 925 °C for 80 h, Tachikawa et al. [40] produced a thick columnar A15 layer with a measured layer composition of 25.3 at.%.

In Fig. 5, we compare the A15 layer (not the overall non-stabilizer J_c in this case) critical current densities of examples of each of the commercially available Nb_3Sn strand geometries, from strands designed for good filament separation for low hysteresis loss application (here model coils from the ITER program), to high J_c ternary PIT strand and high J_c IT designs discussed here. The layer J_c of the best high J_c strand at 12 T is double that of the low hysteresis loss high-Cu designs and approaches the 5500 A/mm^2 figure used to set the 3000 A/mm^2 HEP target.

Fig. 6 compares the microstructures across a sub-element layer from a low hysteresis loss (high-Cu) internal Sn strand with distinctly separated filaments to that of a high J_c strand (both illustrated in Fig. 5) where the initial separated Nb filament structure has converted into one large Nb_3Sn filament that occupies the whole sub-bundle. The grain boundaries revealed by fracture in this figure are the key flux-pinning sites within the Nb_3Sn [41]. However, the images do not explain the difference in layer J_c for these two strands (as shown in Fig. 5), as both the low and high J_c strands have similar, optimized, grain sizes produced by final reaction heat treatments that are at or below 700 °C. The mean Nb_3Sn grain diameter (as calculated from the cross-sectional areas

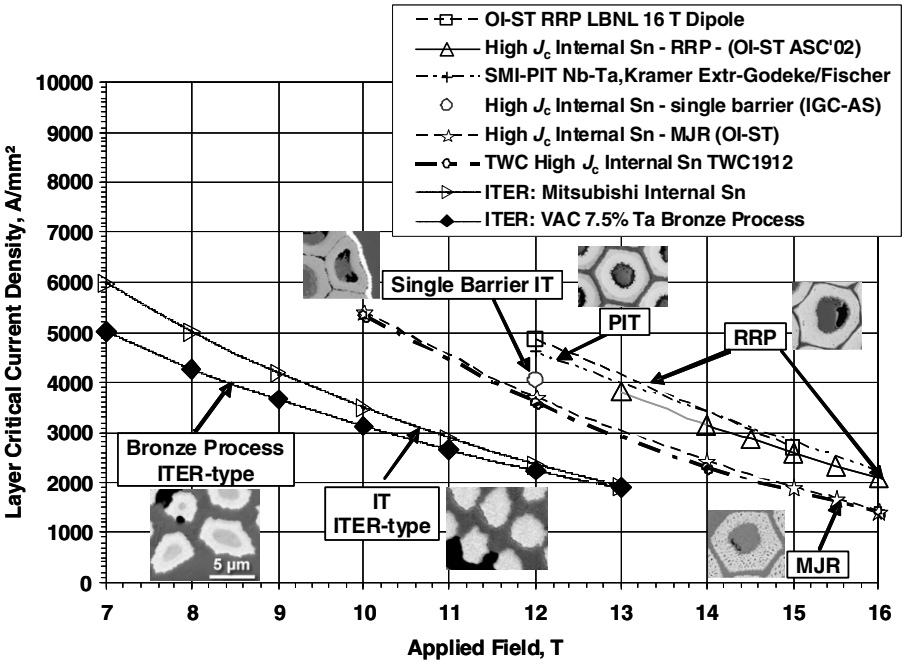

Fig. 5. Variation in Nb_3Sn layer critical current density with applied field for six types of commercial Nb_3Sn strand available in long lengths. The "ITER-type" strands were fabricated for the ITER model coil strand program and are designed to have well separated filaments (and thus low hysteresis loss).

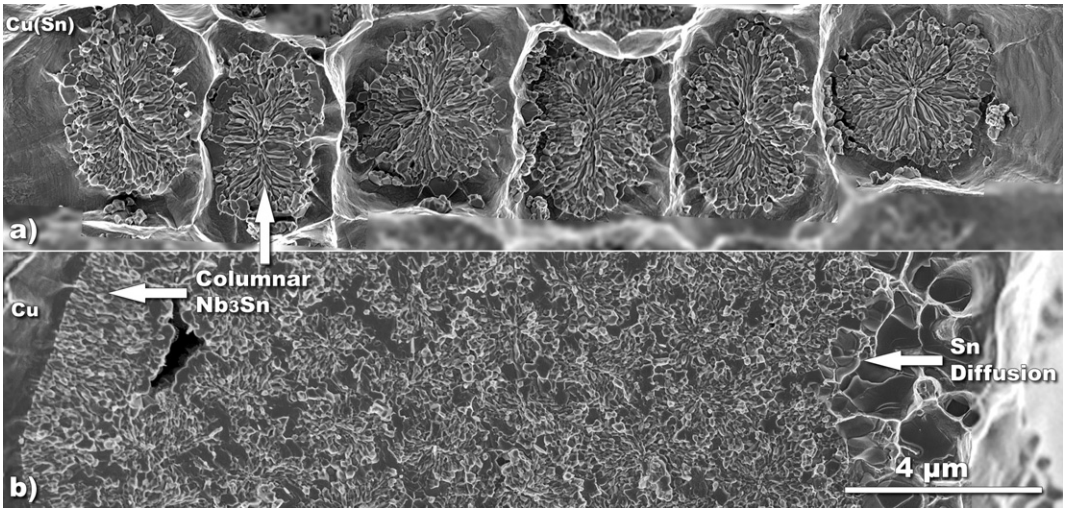

Fig. 6. A comparison between the Nb_3Sn grain microstructures of (a) well separated Nb_3Sn filaments in a low hysteresis loss internal Sn strand ("IT ITER-type" in Fig. 5) with (b) the consolidated Nb_3Sn layer of a "high J_c" Nb_3Sn sub-element (secondary electron SEM image montage). The original Sn source was to the right in both cases and both series of images are to the same scale. Although the A15 grain sizes are similar, there is a pronounced tendency to columnar grain morphology in each of the filaments on (a), whereas columnar grains are only observed at the final reaction interface to the left of (b).

Please cite this article in press as: Lee PJ, Larbalestier DC, Microstructural factors important for the development of high critical current ..., Cryogenics (2008), doi:10.1016/j.cryogenics.2008.04.005

of the grains assuming circularity) for this high-Cu strand increased monotonically filament by filament from 124 nm to 156 nm from the filament nearest the Sn core outwards. In comparison the high J_c layer, even beyond the 4 μm wide large-grain region produced by the liquid Sn–Cu reaction, has a mean grain size close to 165 nm. Additionally the local grain boundary density can be measured, which is more geometrically meaningful than a calculated diameter for columnar grains and from which the specific grain boundary pinning force, Q_{gb}, can be obtained [42]. Interestingly, where the local grain boundary density has been measured it does not change significantly across the equiaxed-to-columnar transition and across the columnar layer towards the center of the filaments where the growing columnar grains impinge upon each other across an ever decreasing reaction interface [42,43]. These results indicate that the density of pinning sites cannot explain the almost twofold difference in J_c between these two strands, rather it is the composition gradient, that controls the T_c and H_{c2} distribution [39]. The essential fact, often overlooked, about Fig. 5, is that the J_c is an average across the whole A15 layer and that the distribution of T_c, H_{c2} and J_c is highly dependent on specific factors of the conductor design.

Comparing the microstructures in Fig. 6, however, another substantial difference is observed in the grain morphology: In the low hysteresis loss filaments the grain morphology switches over from equiaxed to columnar as the reaction proceeds into the core of the Nb filaments, with the columnar grains continuing to grow inwards, restricting each other in lateral growth. In contrast a well defined columnar layer is not observed in high J_c strand, except at the outside interface with the Nb diffusion barrier. In a detailed microchemical and property study of high J_c PIT strands, this changeover from equiaxed to columnar grains was observed to occur after a Sn content drop across the A15 reaction layer of 2.2 at.%Sn [31]. Both H_{c2} and T_c are sensitive to Nb_3Sn composition. Following Devantay et al. [29] a drop in Sn content of 2.2 at.% corresponds to a drop in T_c of almost 4 K. Naus [21] measured both T_c and the irreversibility field, H^* for a variety of high J_c MJR strands as well as a PIT strand manufactured by SMI under a wide range of heat treatments and found a strong linear relationship between T_c and H^*. Using the 4.2 K formula of $H^* = 2.577 \cdot T_c - 17.465$ the 2.2 at.% Sn drop translates into a fall in H^* of almost 10 T. It is not surprising, then, that such large gains in high field critical current can be produced by increasing the Sn content across the entire Nb_3Sn layer. For high J_c strand the average gradient across the A15 layer from core to barrier can be as low as −0.1 at.%Sn/μm [39], however, careful analysis of grain morphology shows that there is still a tendency towards columnar growth as the reaction proceeds in towards the centers of the original filaments that make up the high J_c layer, indicating that local microchemical inhomogeneities still exist despite a low overall gradient across the agglomerated Nb_3Sn layer.

1.4. Ti and Ta alloying

All the high J_c Nb_3Sn strand reviewed here uses Ti or Ta alloying of the Nb_3Sn in order to raise H_{c2} and to improve the critical current density at high field. The work of Suenaga et al. shows that alloying with Ti raises H_{c2} up to a maximum of 27 T (4.2 K) with 2 at.%Ti, followed by a steep drop off, whereas Ta alloying also enhanced to H_{c2} to 27 T but with a broad maximum at ~4.5 at.% [44]. In Bronze Process strand combining both Ta and Ti has been shown to increase the current density at 18 T by 20% over just Ta alloying [11] (the advantage declines with field so that at 15 T there is no benefit and below 15 T the performance is worse). Both Ti- and Ta-alloyed rod have been used successfully to produce high J_c strand.

1.5. In-situ alloying

Alternative methods of introducing the alloying elements are desirable in order to reduce the costs associated with special alloys and to improve the composite mechanical stability by reducing work hardening of the filaments. The Waterbury group used a Ti-alloyed Sn core extensively but obtaining high homogeneity ductile Sn(Ti) cores is costly. Also a collaboration between the Waterbury group, BNL and the Applied Superconductivity Center revealed that a Ti-rich ring (Fig. 7) was produced at the core-filament pack interface early in the heat treatment, hindering the uniform distribution of Sn from the core and producing an inhomogeneous Sn and Ti distribution across the Nb_3Sn layer [45]. A more successful technique for Ti alloying has been the introduction of distributed Nb–47 wt.%Ti alloy rods into the filament pack as a Ti source. An example of the application of distributed Nb–47Ti rods is shown in Fig. 8, where the alloyed rods have been used both as a Ti source and as a method of sub-dividing the sub-element in order to reduce hysteresis loss. Nb–47 wt.%Ti is the dominant commercial superconducting alloy because of its use for magnetic resonance imaging magnets, and is both ductile and homogeneous. An additional benefit observed by OI-ST is that the Ti-doped strand improves the reaction rate and reaction uniformity at the low reaction temperatures (the HT schedule for the LBNL 16 T HD1 magnet was 100 h@210 °C + 48 h@340 °C + 200 h@650 °C) preferred by magnet builders [46,47]. The Nb–47 wt.%Ti technique has reached a level of maturity such that long lengths of >3000 A/mm^2 strand have been produced and it has also been developed as a large production-scale strand for ITER [48].

In Fig. 9, FESEM images of polished cross-sections adjacent to one of the Nb–47Ti rods are shown before and after reaction. Cu-rich islands are found at the original location of the Ti sources and a high Ti region is observed in the Nb_3Sn immediately to the outside of the Cu island. The back-scattered electron image intensity suggests that the source of the high Ti signal is a region of Ti-rich particles ~50 nm in diameter. This is a rare example of a second phase particulate being produced in a Nb_3Sn reaction, offering the possibility that intragrain pinning centers can be introduced into Nb_3Sn. Away from this region energy dispersive X-ray analysis shows a uniform distribution of Ti.

As indicated earlier, combined Ti and Ta alloying is believed to be desirable if the highest fields are to be achieved, however preliminary results on a composite fabricated by OI-ST with Nb(Ta) rods for the filaments and additional Nb–47 wt.%Ti rods for Ti alloying, indicate, as shown in Fig. 10, that the Nb(Ta) alloy rod does not alloy with the distributed Ti as well as in the pure Nb rod case. Ti alloying by insertion of Nb–47Ti rods into the center of the fila-

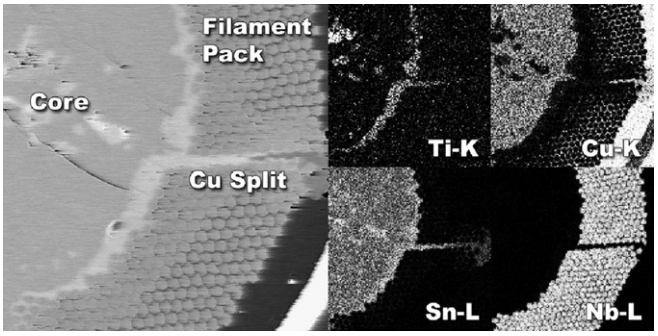

Fig. 7. A rod process internal Sn sub-element using a Ti-alloyed Sn core and a Cu-split for sub-division of the sub-element. EDS spectral images (right) show a Ti–Sn rich layer formed at the edge of the filament pack after 150 h@340 °C heat treatment. Data courtesy of M.C. Jewell as part of a collaboration with M. Suenaga at BNL.

Please cite this article in press as: Lee PJ, Larbalestier DC, Microstructural factors important for the development of high critical current ..., Cryogenics (2008), doi:10.1016/j.cryogenics.2008.04.005

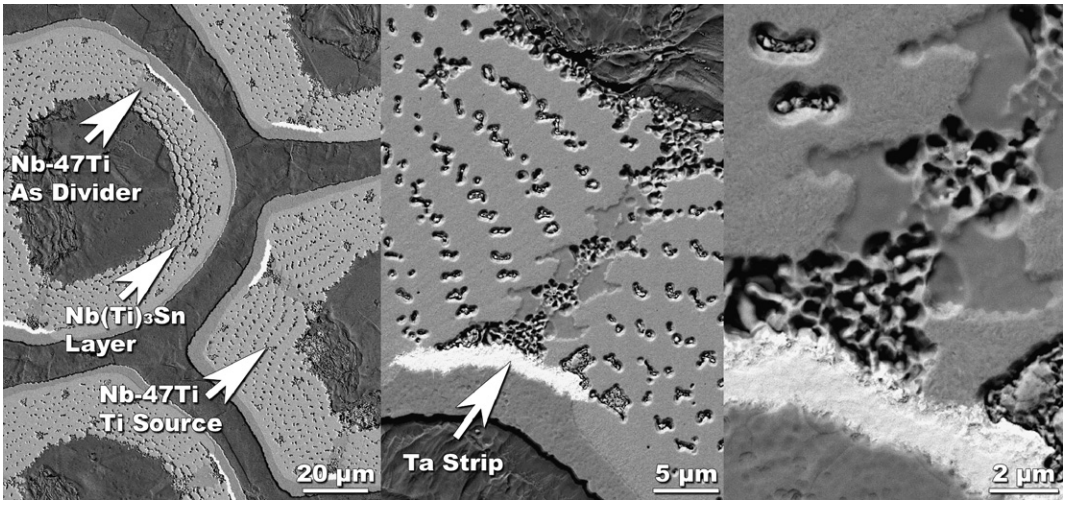

Fig. 8. In this high J_c strand manufactured by OI-ST, Nb–47 wt.%Ti rods are utilized as both a source of Ti for alloying the Nb_3Sn as well as being used in conjunction with Ta foil to sub-divide the sub-element. In this series of electron backscatter images at increasing magnification, the Cu-rich regions have been preferentially etched by an Ar ion beam revealing a Nb_3Sn-free region where the Nb–47Ti rods has been located. Arrows indicate positions of the Nb–47Ti rods before reaction.

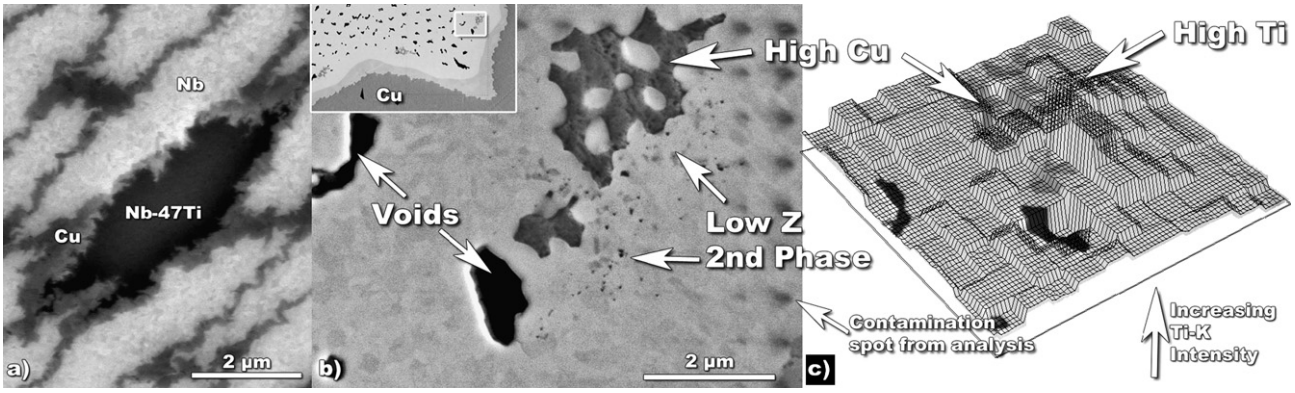

Fig. 9. OI-ST distributed Nb–47Ti rod processed internal Sn, (a) before heat treatment and (b)–(c) after heat treatment. The original Sn source is from the direction of the top left hand corner. After heat treatment, Cu-rich islands are located at the original positions of the Nb–47Ti rods. Atomic number sensitive FESEM-BEI image (b) reveals low atomic number 2nd phase with ~50 nm diameter on the outer side of the Cu-rich islands only. In (c) a height map generated from the Ti–K Energy Dispersive X-ray analysis is superimposed on the analysis region and indicates that a high Ti region is co-incident with the 2nd phase dispersion.

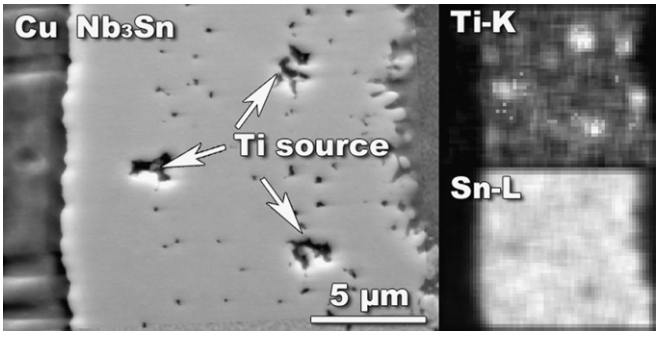

Fig. 10. The right images show Ti–K and Sn–L EDS maps for a $Nb(Ta)_3Sn$ OI-ST composite strand sub-element layer (left). High Ti levels remain at the original locations of the Nb–47Ti rods suggesting that the Ti redistribution is not uniform in this design.

ments prior to assembly [49] has been has recently been the subject of a detailed comparative study of alloying methods for Nb–7.5Ta based Bonze-process strands at the University of Geneva [36] where it was found to suppress J_c yet produced similar grain sizes and Ti distributions to that achieved by doping with Ti alloyed bronze.

2. Issues with high J_c designs

2.1. Effective filament diameter

Because there is insufficient Cu in high J_c designs to separate the Nb filaments, they react together to form a tube of Nb_3Sn around the original core, making the effective filament diameter the sub-element diameter. For typical 61 sub-element designs, the ~70–120 μm diameter is too large for stable magnet operation [22]. Two approaches have been adopted to reduce the effective filament diameter to 40 μm or less, first by internal sub-division of the sub-elements [50], as shown in Fig. 8, and second by reducing the sub-element size before stacking. By using a 127 element stack, the sub-element diameter can be reduced to ~49 μm for a 0.7 mm diameter final wire size [50]. However, it has also been the experience of OI-ST that the piece length decreases as the number of sub-elements increases [50].

A combination of pure Ta rods and sheets was used by OI-ST [50] to sub-divide each sub-element shown in Fig. 11. The magneto optical image shown in the right hand overlay in Fig. 11 shows that the Ta rods have successfully sub-divided the sub-element but the significant T_c variations are indicative of the Ta barriers restricting the uniform distribution of the Sn throughout the sub-element.

Please cite this article in press as: Lee PJ, Larbalestier DC, Microstructural factors important for the development of high critical current ..., Cryogenics (2008), doi:10.1016/j.cryogenics.2008.04.005

The effectiveness of sub-division by this technique has been demonstrated by magnetization measurement [51] which showed a D_{eff} of 42 μm compared to the original sub-element diameter of 88 μm. Ta has a couple of significant disadvantages, however. First, Ta work hardens much faster than other elements in the composite and can lead to significant reduction in yield. Second, the Ta reacts with the Sn, both reducing the available Sn for the Nb_3Sn reaction and creating a low T_c (~7 K), low H_{c2} (5 T at 4.5 K) superconducting phase [52] that still can couple the whole sub-bundle at low field [51]. Given the additional problems of strong work hardening through multiple extrusions and the high cost of Ta, it is desirable to eliminate or at least minimize the amount of Ta used. Consequently OI-ST are exploring the use of Nb–47Ti rods as dividers and Ti sources as shown in Fig. 8 [46].

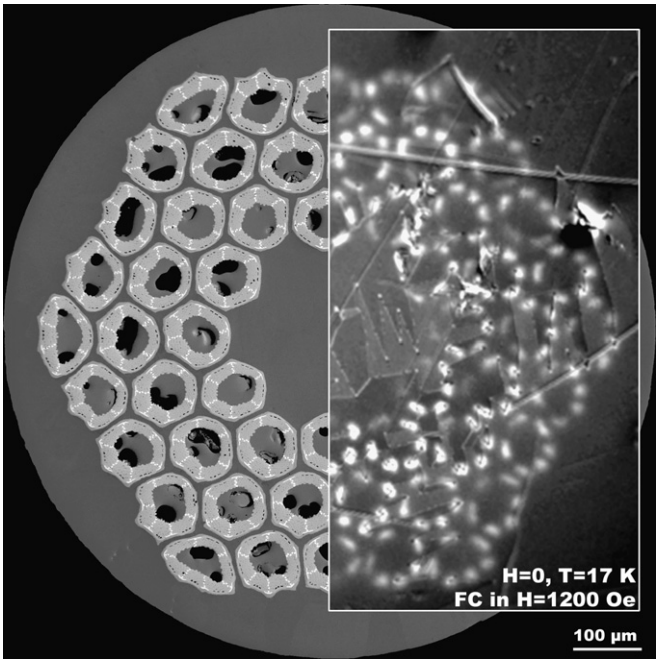

Fig. 11. T_c variation in Ta rod sub-divided sub-elements revealed by a magneto optical image. The MO image (overlaid onto an electron backscatter image to the same scale) reveals variations in T_c from sub-element to sub-element and from one sub-divided area to another. MO imaging by Anatolii Polyanskii.

2.2. Barrier breakdown and Cu poisoning

Although the first indications for the high field accelerator magnet performance looked very good [53] (even though it was clear that the excess Sn had resulted in complete reaction through the Nb diffusion barrier into the Cu stabilizer), some intermediate field magnets (10–12 T) [54,55] were unstable when Sn poisoning of Cu occurred. For intermediate field magnets, backing away from the highest J_c, reducing the D_{eff}, and producing a higher RRR, has been more effective. [56] It has also been noticed that high J_c strands can also be sensitive to cable degradation [57–59]. For these and various other reasons, such as cost and suitability for local fabrication capabilities, Nb_3Sn conductors are still subject to much design evolution in the search towards the highest J_c, H_{c2} and the smallest filament size, all in an affordable and fabricable package.

2.3. Strain sensitivity of large filament masses

A very active area of present interest is that of fracture sensitivity of Nb_3Sn strands due to the significant cyclic damage that can occur in some designs of cable-in-conduit conductor [60,61] when large unsupported bend strains occur. It has long been known that high area fractions of superconductor reduce the pre-strain that provides essential compressive stresses around the brittle Nb_3Sn phase [62]. Not only do the modern high J_c strands have higher niobium fractions and smaller Cu contents than low hysteresis loss, lower J_c strand designs but they also have very large bonded filament diameters (~40–120 μm) so that the detrimental effects of bend strain are magnified compared to discrete filament conductors with 5 μm or smaller filament diameters. The comparative sensitivity of different conductor designs to fracture under bend strain was observed by Jewell et al. [63]. An example of the great increase in fracture damage possible in large filament strands characteristics of high J_c agglomerated strands is shown in Fig. 12. After a bend strain of only 0.5% (relative to the wire diameter), the Nb_3Sn layers on the tensile side of the bend have completely fractured. But it is also clear that the fracture has not propagated into the compressive side of the strand. This area is one of great present interest due to the cyclic strain-related effects seen in some ITER

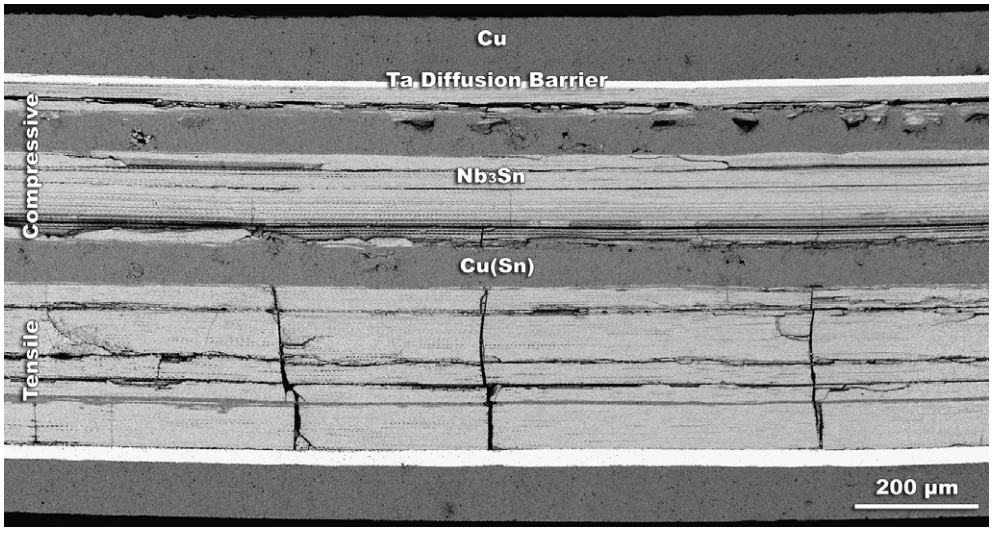

Fig. 12. Polished longitudinal cross-section of prototype rod process single barrier high J_c strand, manufactured by IGC-AS, after 0.5% bend strain at room temperature. On the tensile side of the strand the Nb_3Sn sub-elements have been fractured across their entire width.

Please cite this article in press as: Lee PJ, Larbalestier DC, Microstructural factors important for the development of high critical current ..., Cryogenics (2008), doi:10.1016/j.cryogenics.2008.04.005

prototype conductors and to the need to control them. Many years of excellent performance in both solenoidal and saddle magnets have shown that Nb_3Sn fracture is a fully controllable problem. What recent ITER conductors are showing is that the unsupported crossovers in open cables can lead to excessive bending strains that can lead to damage under large cyclic Lorentz loads [64,65]. This is focusing attention on key parameters of the cable design, such as void fraction, twist pitch and cable lay up parameters, as well as those of the conductor itself [66]. In additional to the parameters already discussed, we also should recall the work of Ekin and co-workers who showed that addition of dispersion-strengthened copper into the matrix could be used to increase the pre-strain to higher levels [67].

3. The future

The new designs of high J_c Nb_3Sn strands discussed here have shown that the major roadblock to high critical current density in Nb_3Sn strands is attaining high Sn levels throughout the A15 layer, which in fact only has Nb_3Sn composition near the Sn source-A15 phase reaction interface. However, a fine grain size is still beneficial to J_c but so far the A15 grain size in existing composites remains at the 100–150 nm scale. Such a grain size means that there are far fewer pinning sites than vortices (at 15 T the vortex spacing is 12 nm) making the desire for intragrain pinning centers still relevant. A proof of principle of the value of denser pinning centers has been shown by Cooley et al. who showed a significant upward shift in the field at which the maximum pinning force occurs for PIT strand with a very fine grain size of 57 nm [68]. However such fine grains can only be attained with low temperature reactions that also have large Sn gradients, thus emphasizing the value of approaches using precipitates or interstitials to limit grain boundary growth (e.g. [69]). Fig. 4 makes it clear that T_c and H^* can be pushed to higher levels with higher temperature heat treatments. The only present detriment to such treatments is the grain growth that they produce, making control of grain size perhaps the next valuable area on which to focus in the pursuit of very higher critical currents. Enhanced J_c is certainly feasible in Nb_3Sn because of the dilute nature of the pinning center distribution, much smaller than is the case for Nb–Ti [70]. Dietderich and Scanlan have shown significant improvement in J_c with pinning center additions by doping thin film Nb_3Sn [15] and this remains an area that has not been explored for high J_c strands.

4. Summary

Considering the long history of Nb_3Sn, it is remarkable how much progress has been made since 1999. Amongst the highlights we can cite:

1. 3000 A/mm^2 at 12 T and 4.2 K is achieved in long production lengths of strand.
2. The strand has been used to fabricate an accelerator-type magnet design operating at >16 T.
3. Radial Sn gradients across wide A15 layers have been reduced to an average of −0.1 at.%Sn/μm.
4. Effective low cost alloying has been demonstrated using distributed Nb–47Ti rods.
5. Sub-division of and increasing sub-element stacking have shown progress towards effective filament diameters of <40 μm.

With major driving forces to higher-field deriving from the race for 1 GHz NMR (23.5 T) and the next generation of magnets for High Energy Physics as well as the experience of large quantity production for ITER, the expectation is that Nb_3Sn will continue to see improvements in performance and reductions in cost.

Acknowledgements

Long term support for this work at the Applied Superconductivity Center has been supplied by the US Department of Energy through the Division of High Energy Physics (DE-FG02-07ER41451) and Office of Fusion Energy Science (DE-FG02-06ER54881). Several of our graduate students have made important contributions to our efforts to understand the limitations to Nb_3Sn strand performance: Christopher Hawes, Chad Fischer, Arno Godeke, Matthew Jewell and Michael Naus. Finally we would like to thank the participants of the Low Temperature Superconductor Workshop, which for 25 years has brought together industry, universities and national laboratories to push the performance limits of superconductor technology for the high energy physics community.

References

[1] Takeuchi T et al. Status and perspective of the Nb_3 Al development, this issue. doi:10.1016/j.cryogenics.2008.04.007.
[2] Suenaga M. Understanding properties and fabrication processes of superconducting Nb_3Sn wires: progress. In: Timmerhaus KD, Reed RP, editors. Cryogenic engineering: fifty years of progress. Series: international cryogenics monograph series. New York: Springer; 2007.
[3] Godeke A. A review of the properties of Nb_3Sn and their variation with A15 composition, morphology and strain state. Supercond Sci Technol 2006;19: R68–80.
[4] Hornsveld EM, Elen JD, van Beijnen CAM, Hoogendam P. Development of ECN-type Nb_3Sn wire towards smaller filament size. Adv Cryogenic Eng 1987;34: 493–8.
[5] den Ouden A, Wessel S, Krooshoop E, ten Kate H. Application of Nb_3Sn superconductors in high-field accelerator magnets. IEEE Trans Appl Supercond 1997;7(2):733–8.
[6] Lindenhovius JH, Hornsveld EM, den Ouden A, Wessel WAJ, ten Kate HHJ. Progress in the development of Nb_3Sn conductors based on the "Powder in Tube" method with finer filaments. IEEE Trans Appl Supercond 1999;9(2): 1451–4.
[7] Godeke A. State of the art Powder-in-Tube Nb_3Sn superconductors. IEEE Trans Appl Supercond 1999;9(2):1451–4.
[8] Lee PJ, Fischer CM, Naus MT, Jewell MC, Squitieri AA, Larbalestier DC. The microstructure and micro-chemistry of high critical current Nb_3Sn strands manufactured by the bronze, internal-Sn and PIT techniques. IEEE Trans Appl Supercond 2003;13(2):3422–5.
[9] Hashimoto Y, Yoshizaki K, Tanaka M. In: Mendelssohn K, editor. Proceedings of the 5th ICEC, Kyoto 1974, Vol. 332. London: IPC Science and Technology Press; 1974.
[10] Pyon T, Gregory E. Niobium–tin for fusion, high energy physics and other applications. IEEE Trans Appl Supercond 1999;9(2):2509–12.
[11] Zhang Y, McKinnell JC, Hentges RW, Hong S. Recent development of niobium–tin superconducting wire at OST. IEEE Trans Appl Supercond 1999;9(2:2):1444–6.
[12] Scanlan RM. Conductor development for high energy physics-plans and status of the US program. IEEE Trans Appl Supercond 2001;11(I):2150–5.
[13] Lee PJ, Squitieri AA, Larbalestier DC. Nb_3Sn: macrostructure, microstructure, and property comparisons for bronze and internal Sn process strands. IEEE Trans Appl Supercond 2000;10(1):979–82.
[14] Zeitlin BA, Gregory E, Pyon T. A high current density low cost Niobium(3)Tin conductor scalable to modem niobium titanium production economics. IEEE Trans Appl Supercond 2001;11(1:3):3683–7.
[15] Dietderich DR, Scanlan RM. Nb_3Sn artificial pinning microstructures. IEEE Trans Appl Supercond 1997;7(2:2):1201–4.
[16] Cooley LD, Ghosh AK, Scanlan RM. Costs of high-field superconducting strands for particle accelerator magnets. Supercond Sci Technol 2005;18(4):R51–65.
[17] Parrell JA, Zhang Y, Field MB, Hong S. Nb_3Sn strand development at Oxford Superconducting Technology. Presentation at the Low Temperature Superconductor Workshop, November 12–14, 2001, Marriott Napa Valley, California.
[18] Parrell JA, Zhang Y, Field MB, Cisek P, Hong S. High field Nb_3Sn conductor development at Oxford Superconducting Technology. IEEE Trans Appl Supercond 2003;13(2):3470–3.
[19] Murase S, Koizumi M, Horigami O, Shiraki H, Koike Y, Suzuki E, et al. Multifilament niobium–tin conductors. IEEE Trans Magnetics 1979;MAG15(1): 83–6.
[20] Naus MT, Lee PJ, Larbalestier DC. The influence of the starting Cu–Sn phase on the superconducting properties of subsequently reacted internal-Sn Nb_3Sn conductors. IEEE Trans Appl Supercond 2001;11(1:3):3569–72.

[21] Naus MT. Optimization of internal-Sn Nb_3Sn composites. PhD thesis, The University of Wisconsin-Madison, 2002.
[22] Ghosh AK, Sperry EA, Cooley LD, Moodenbaugh AM, Sabatini RL, Wright JL. Dynamic stability threshold in high-performance internal-tin Nb_3Sn superconductors for high field magnets. Supercond Sci Technol 2005;18:L5–8.
[23] Bordini B, Barzi E, Feher S, Rossi L, Zlobin AV. Self-field effects in magneto-thermal instabilities for Nb–Sn strands. IEEE Trans Appl Supercond 2008;18(2):1309–12.
[24] Pyon T, Gregory E. Nb_3Sn conductors for high energy physics and fusion applications. IEEE Trans Appl Supercond 2001;11(1:3):3688–91.
[25] Gregory E, Pyon T. Internal tin Nb_3Sn conductor development for high energy physics application. Adv Cryogenic Eng 2002;48B:958–67.
[26] Pyon T, Kanithi H. Development of Nb_3Sn conductors for fusion and high energy physics. IEEE Trans Appl Supercond 2003;13(2):3474–7.
[27] Benjegerdes R et al. Fabrication and test results of a high field, Nb_3Sn superconducting racetrack dipole magnet. In: Proceedings of the 2001 particle accelerator conference, Chicago, IL, June 2001, Pub. IEEE Conference Series, vol. 1, 18–22 June 2001. p. 208–10.
[28] Hafalia AR et al. HD-1: 16 T, Nb_3Sn dipole magnet design and fabrication. IEEE Trans Appl Supercond 2004;14(2):283–6.
[29] Devantay H, Jorda JL, Decroux M, Muller J, Flükiger R. The physical and structural properties of superconducting A15-type Nb–Sn alloys. J Mater Sci 1981;16(8):2145–53.
[30] Jewell MC, Godeke A, Lee PJ, Larbalestier DC. The upper critical field of stoichiometric and off-stoichiometric bulk, binary Nb_3Sn. Adv Cryogenic Eng 2004;50(B):474–81.
[31] Hawes CD, Lee PJ, Larbalestier DC. Measurements of the microstructural, microchemical and transition temperature gradients of A15 layers in high performance Nb_3Sn PIT superconducting strand. Supercond Sci Technol 2006;19:S27–37.
[32] Fischer CM, Lee PJ, Larbalestier DC. Irreversibility field and critical current density as a function of heat treatment time and temperature for a pure niobium Powder-in-Tube Nb_3Sn conductor. Adv Cryogenic Eng 2002;48(B):1008–15.
[33] Cooley LD, Fischer CM, Lee PJ, Larbalestier DC. Simulations of the effects of tin composition gradients on the superconducting properties of Nb_3Sn conductors. J Appl Phys 2004;96(4):2122–30.
[34] Smathers D, Marken K, Larbalestier D, Evans J. Scanning Auger investigation of commercial multifilamentary Nb_3Sn conductors. IEEE Trans Magnetics 1983;19(3):1421–4.
[35] Wu IW, Dietderich DR, Holthuis JT, Hong M, Hassenzahl WV, Morris Jr JW. The microstructure and critical current characteristic of a bronze-processed multifilamentary Nb_3Sn superconducting wire. J Appl Phys 1982;54(12):7139–52.
[36] Abächerli V, Uglietti D, Lezza P, Seeber B, Flükiger R, Cantoni M, et al. The influence of Ti doping methods on the high field performance of $(Nb, Ta\ Ti)_3Sn$ multifilamentary wires using Osprey bronze. IEEE Trans Appl Supercond 2005;15(2):3482–5.
[37] Uglietti D, Abächerli V, Cantoni M, Flükiger R. Grain growth, morphology, and composition profiles in industrial Nb_3Sn wires. IEEE Trans Appl Supercond 2007;17(2:3):2615–8.
[38] Godeke A, Jewell MC, Fischer CM, Squitieri AA, Lee PJ, Larbalestier DC. The upper critical field of filamentary Nb_3Sn conductors. J Appl Phys 2005:97–9. article number 093909.
[39] Lee PJ, Larbalestier DC. Microstructure, microchemistry and the development of very high Nb_3Sn layer critical current density. IEEE Trans Appl Supercond 2005;15(2):3474–7.
[40] Tachikawa K, Yamamoto S, Yokoyama T, Kato T. New high-field Nb_3Sn conductors prepared from Ta–Sn compound powder. IEEE Trans Appl Supercond 1999;9(2:2):2500–4.
[41] Scanlan RM, Fietz WA, Koch EF. J Appl Phys 1975;46:2244–9.
[42] Lee PJ, Ruess JR, Larbalestier DC. Quantitative image analysis of filament coupling and grain size in ITER $Nb(Ti)_3Sn$ strand manufactured by the internal Sn process. IEEE Trans Appl Supercond 1997;7(2:2):1516–9.
[43] Lee PJ, Larbalestier DC. Compositional and microstructural profiles across Nb_3Sn filaments produced by different fabrication methods. IEEE Trans Appl Supercond 2001;11(1:3):3671–4.
[44] Suenaga M, Welch DO, Sabatini RL, Kammerer OF, Okuda S. J Appl Phys 1986;59:840–53.
[45] Suenaga M, Gregory E, Pyon T, Jewell MC, Ulrich J, Lee PJ, et al. unpublished.
[46] Field MB, Parrell JA, Zhang Y, Hong S. Nb_3Sn conductor development for fusion and particle accelerator applications. Adv Cryogenic Eng 2005;52(B):544–9.
[47] Lietzke AF et al. Test results for HD1, a 16 T Nb_3Sn dipole magnet. IEEE Trans Appl Supercond 2004;14:345–8.
[48] Field MB, Parrell JA, Zhang Y, Meinesz M, Hong S. Internal tin Nb_3Sn conductors for particle accelerator and fusion applications. Adv Cryogenic Eng 2008;54:237–43.
[49] Nikulin A, Shikov A, Vorobjova A, Khlebova N, Malafeeva O, Pantsyrnyi V, et al. The investigation of the effect of niobium artificial doping with titanium on Nb_3Sn superconductors properties. Adv Cryogenic Eng 1996;42:1337–43.
[50] Parrell JA, Field MB, Zhang YA, Hong S. Advances in Nb_3Sn strand for fusion and particle accelerator applications. IEEE Trans Appl Supercond 2005;15(2:2):1200–4.
[51] Ghosh AK, Cooley LD, Moodenbaugh AR, Parrell JA, Field MB, Zhang Y, et al. Magnetization studies of high J_c Nb_3Sn strands. IEEE Trans Appl Supercond 2005;15(2):3494–7.
[52] Otto G. Preparation and properties of Ta–Sn and Nb–Ge diffusion layers. J Appl Phys 1971;42(1):57.
[53] Lietzke AF et al. Test results on HD 1b, an upgraded 16 Tesla dipole magnet. IEEE Trans Appl Supercond 2005;15(2):1123–7.
[54] Zlobin AV et al. R&D of Nb_3Sn accelerator magnets at Fermilab. IEEE Trans Appl Supercond 2005;15(2):1113–8.
[55] Ghosh AK, Cooley LD, Parrell JA, Field MB, Zhang Y, Hong S. Effects of reaction temperature and alloying on performance of restack-rod-process Nb_3Sn. IEEE Trans Appl Supercond 2007;17(2:3):2623–6.
[56] Barzi E, Del Frate L, Turrioni D, Zlobin AV. Effect of temperature and deformation on Nb_3Sn strands instabilities. Adv Cryogenic Eng 2006;52(B):566–74.
[57] Barzi E for the HFM group. Properties of modern Nb_3Sn strands and cables. Workshop on Accelerator Magnet Design and Optimization, CERN 3–6 April 2006.
[58] Turrioni D, Barzi E, Bossert M, Kashikhin VV, Kikuchi A, Yamada R, et al. Study of effects of deformation in Nb_3Sn multifilimentary strands. IEEE Trans Appl Supercond 2007;17(2:3):2710–3.
[59] Dietderich DR, Higley HC, Scanlan RM. Design and fabrication of Rutherford-type cables for high field magnets. Workshop on Accelerator Magnet Design and Optimization, CERN 3–6 April 2006.
[60] Mitchell N. Mechanical and magnetic load effects in Nb_3Sn cable-in-conduit conductors. Cryogenics 2003;43:255–70.
[61] Nijhuis A, Ilyin Y, Abbas W, Ten Haken B, Ten Kate HHJ. Performance of an ITER CS1 model coil conductor under transverse cyclic loading up to 40,000 cycles. IEEE Trans Appl Supercond 2004;14(2):1489–94.
[62] Ekin JW. Strain effects in superconducting compounds. Adv Cryogenic Eng 1984;30:823–36.
[63] Jewell MC, Lee PJ, Larbalestier DC. The influence of Nb_3Sn strand geometry on filament breakage under bend strain as revealed by metallography. Supercond Sci Technol 2003;16:1005–11.
[64] Nijhuis A, De Rapper WM. Solution for Lorentz forces response and degradation in Nb3Sn Cable in Conduit Conductors; verification of cabling effect. IEEE Trans Appl Supercond 2008;18(2):1491–95.
[65] Nijhuis A, Ilyin Y, Abbas W, Wessel WAJ, Krooshoop HJG. Performance of ITER (EU-TFPRO-2) Nb3Sn strands under spatial periodic bending, axial strain and contact stress. IEEE Trans Appl Supercond 2008;18(2):1059–62.
[66] Bessette D, Mitchell N. Review of the results of the ITER toroidal field conductor R&D and qualification. IEEE Trans Appl Supercond 2008;18(2):1109–13.
[67] Ekin JW, Cheggour N, Abrecht M, Clickner C, Field M, Hong S, et al. Compressive pre-strain in high-niobium-fraction Nb_3Sn superconductors. IEEE Trans Appl Supercond 2005;15(2):3560–3.
[68] Cooley LD, Lee PJ, Larbalestier DC. Changes in flux pinning curve shape for flux-line separations comparable to grain size in Nb_3Sn wires. Adv Cryogenic Eng 2002;48(B):925–32.
[69] Zeitlin BA, Gregory E, Marte J, Benz M, Scanlan R, Dietderich D. The effect on the superconducting properties of the addition of oxygen and titanium to $(Nb1Zr)_3Sn$ Mono Element Internal Tin (MEIT) conductors. Adv Cryogenic Eng 2006;52(B):513–9.
[70] Meingast C, Lee P, Larbalestier D. Quantitative description of a high J_c Nb–Ti superconductor during its final optimization strain: I. microstructure, T_c, H_{c2}, and resistivity. J Appl Phys 1989;66(12):5962–70.

Please cite this article in press as: Lee PJ, Larbalestier DC, Microstructural factors important for the development of high critical current ..., Cryogenics (2008), doi:10.1016/j.cryogenics.2008.04.005